ACS APPLIED MATERIALS & INTERFACES

Research Article

www.acsami.org

Origin of Electrochemical, Structural, and Transport Properties in Nonaqueous Zinc Electrolytes

Sang-Don Han,[†,‡,⊥] Nav Nidhi Rajput,[†,§,⊥] Xiaohui Qu,[†,§] Baofei Pan,[†,‡] Meinan He,[‡,∥] Magali S. Ferrandon,[†,‡] Chen Liao,[†,‡] Kristin A. Persson,[*,†,§] and Anthony K. Burrell[*,†,‡]

[†]Joint Center for Energy Storage Research, Argonne National Laboratory, Lemont, Illinois 60439, United States

[‡]Chemical Sciences and Engineering Division, Argonne National Laboratory, Lemont, Illinois 60439, United States

[§]Environmental Energy Technologies Division, Lawrence Berkeley National Laboratory, Berkeley, California 94720, United States

[∥]Department of Mechanical Engineering, Worcester Polytechnic Institute, Worcester, Massachusetts 01609, United States

Supporting Information

ABSTRACT: Through coupled experimental analysis and computational techniques, we uncover the origin of anodic stability for a range of nonaqueous zinc electrolytes. By examination of electrochemical, structural, and transport properties of nonaqueous zinc electrolytes with varying concentrations, it is demonstrated that the acetonitrile–$Zn(TFSI)_2$, acetonitrile–$Zn(CF_3SO_3)_2$, and propylene carbonate–$Zn(TFSI)_2$ electrolytes can not only support highly reversible Zn deposition behavior on a Zn metal anode (≥99% of Coulombic efficiency) but also provide high anodic stability (up to ~3.8 V vs Zn/Zn^{2+}). The predicted anodic stability from DFT calculations is well in accordance with experimental results, and elucidates that the solvents play an important role in anodic stability of most electrolytes. Molecular dynamics (MD) simulations were used to understand the solvation structure (e.g., ion solvation and ionic association) and its effect on dynamics and transport properties (e.g., diffusion coefficient and ionic conductivity) of the electrolytes. The combination of these techniques provides unprecedented insight into the origin of the electrochemical, structural, and transport properties in nonaqueous zinc electrolytes.

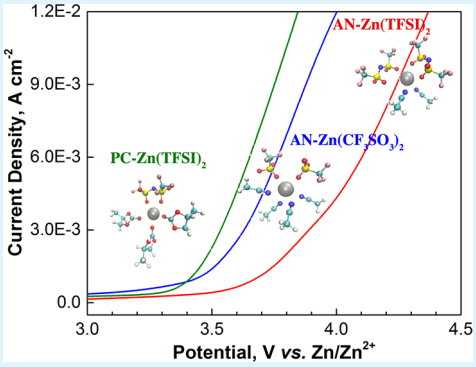

KEYWORDS: *nonaqueous electrolyte, electrode/electrolyte interface, reversible deposition, Coulombic efficiency, anodic stability, solvation structure*

INTRODUCTION

Electrochemical, structural, and transport properties of an electrolyte play a crucial role in defining the performance characteristics of energy storage technologies (e.g., batteries, fuel cells, and supercapacitors), sensors, metal plating, and many other applications.[1−7] Thus, it is of paramount importance to obtain fundamental understanding of electrolyte properties and behavior that govern (in part) application performance. The electrolytes, however, remain a poorly understood topic relative to the research devoted to other components and have undergone only minor changes for a long time holding back the progression of those applications. For example, the Li-ion battery, one of the most promising energy storage technologies, has been developed for the past 30 years mostly focusing on the electrodes and recently the electrode/electrolyte interface, but it still faces several issues (limited performance, cost, aging, and safety concerns which are mostly induced from limitation of the current state-of-the-art electrolyte) to apply in transportation and the electricity grid. With constant inflation in energy generation the future energy storage quest is rapidly moving toward high performance, safe and low cost batteries such as metal−air, multivalent, and lithium−sulfur batteries, but the development of a comprehensive understanding of electrolyte interactions/properties and the exploration of new electrolyte solvents/salts are required to advance beyond Li-ion battery technologies.

As one of the potential candidates for a post-lithium-ion battery, nonaqueous multivalent (e.g., Mg^{2+}, Ca^{2+}, and Zn^{2+}) metal cells provide an attractive opportunity in energy storage research due to higher theoretical volumetric capacity of a multivalent metal anode and the limited dendrite formation at the Mg metal anode.[8] The development of compatible multivalent electrolytes with a metal anode and reversible multivalent intercalation cathodes, however, is a significant challenge requiring an increased focus on fundamental understanding of electrolyte properties and behavior. For instance, in Mg metal cells various halides, halide derivatives, BH_4, and BH_4 derivatives electrolytes are known to be compatible with Mg metal anode, but correlation between speciation and functionality is still under debate.[9−21] The compatibility of glyme–$Mg(TFSI)_2$ electrolyte with Mg metal is also controversial, and generally a high overpotential and low

Received: October 20, 2015
Accepted: January 12, 2016

DOI: 10.1021/acsami.5b10024
ACS Appl. Mater. Interfaces XXXX, XXX, XXX−XXX

Coulombic efficiency are observed in cell cycling.[21,22] In the case of Ca metal cells, an electrolyte has been recently developed that has some reversible chemistry at a Ca metal anode, however, there still needs to be substantial improvement for practical implementation.[23,24] We note that Ca has a very low standard free energy of oxide formation, lower even than Mg metal, compared to other metals as noted in a Ellingham diagram.[25] However, it appears that Zn^{2+} ion chemistry in Zn metal cells provides an exception among multivalent metals. Zn metal anodes coupled with a reversible intercalation cathode chemistry have a number of promising features: (1) highly efficient (≥99%) reversible Zn deposition on Zn metal anode in high performance nonaqueous Zn electrolytes (e.g., high anodic stability (maximum ∼3.8 V) and ionic conductivity); (2) relatively lower activation barrier energy for migration of Zn^{2+} ions in a variety of cathode materials (e.g., $FePO_4$, NiO_2, and V_2O_5);[26] (3) similar ionic radius compared with Li^+ and Mg^{2+} ions;[27] (4) much higher volumetric capacity compared to other multivalent metals, such as Mg and Ca.[8] However, due to the high electrochemical potential of Zn metal, Zn cells are not considered a competitor compared to Li-ion energy storage. Nevertheless, the nonaqueous Zn system provides an opportunity to delve into the mechanisms in multivalent cell chemistry (e.g., reversible deposition on a metal anode and (de)intercalation into (from) a cathode material) and furthermore possibly solves the present issues in multivalent cell design and prototyping. From previous studies, it is apparent that the advent of multivalent batteries relies on the electrochemical, transport, and structural properties of electrolytes. An enhanced understanding of nonaqueous Zn electrolyte (electrochemical and transport properties (e.g., anodic stability, diffusion coefficient, and ionic conductivity) and mechanisms at an electrolyte/electrode interface) can aid in understanding the correlation between the atomistic structure of the electrolyte and its performance by utilizing experimental analysis combined with classical molecular dynamics and DFT calculations. As shown in previous studies,[28−34] the molecular-level solvation structure (i.e., ion solvation and ionic association behavior) and dynamics of the bulk electrolytes are not only crucial factors influencing the bulk electrolyte properties and possibly elucidating mechanisms at an electrolyte/electrode interface but also critical design metrics for novel electrolytes.

Most of the previous rechargeable Zn cell studies have been performed using aqueous Zn electrolytes, such as $Zn(NO_3)_2$ and/or $ZnSO_4$, with various types of MnO_2 or copper hexacyanoferrate (CuHCF) nanocube cathodes, which mostly focus on the structural and electrochemical properties of cathode materials, reversible intercalation mechanism, and cycle life performance for the Zn metal cells.[35−41] On the other hand, in 1987 R. Schöllhorn et al. reported the intercalation of Zn^{2+} ion by electron/ion transfer reactions into the Chevrel-type molybdenum cluster chalcogenides Mo_6X_8 (X = S, Se) in nonaqueous electrolytes (i.e., $Zn(ClO_4)_2$ in acetonitrile (AN) or propylene carbonate (PC)) demonstrating the competitive influence of electronic and steric factors upon these processes.[42] As new rechargeable Zn electrolytes, the binary room temperature molten electrolyte based on acetamide and $Zn(ClO_4)_2$[43] and the dicyanamide ionic liquids-based electrolytes[44] were characterized and evaluated with the γ-MnO_2/Zn and Zn/Zn cells, respectively. K. Zaghib et al. recently demonstrated cycling performance of a Zn/PANi (polyaniline) cell with a nonaqueous PC−$Zn(TFSI)_2$ electrolyte.[45] Remarkably, most previous studies on Zn^{2+} ion (de)intercalation mechanism or rechargeable Zn battery have been performed in aqueous Zn electrolyte system, while very little information is available in the literature on nonaqueous Zn battery, in particular nonaqueous Zn electrolytes.

Hence, this study aims to scrutinize in detail the general electrochemical and transport properties (e.g., reversible Zn metal deposition behavior with Coulombic efficiency, overpotential, anodic stability, diffusion coefficient, and ionic conductivity) of nonaqueous Zn electrolytes consisting of mixtures of Zn salts (e.g., $Zn(PF_6)_2$, $Zn(TFSI)_2$, $Zn(BF_4)_2$, and $Zn(CF_3SO_3)_2$) and organic solvents (e.g., diglyme, propylene carbonate, acetonitrile, and *N*,*N*-dimethylformamide). Classical molecular dynamics simulations are utilized to complement the experimental work and to provide insights into the molecular-level ion solvation/ionic association behavior, dynamics of the bulk electrolytes, and the relationship between solution structure and transport properties of bulk electrolytes. In addition, electrochemical stability windows of the electrolytes are predicted via adiabatic ionization potential (IP) DFT calculations considering both solvents and salt anions.

EXPERIMENTAL AND COMPUTATIONAL METHODS

Materials and Electrolyte Preparation. The zinc salts and solvents used in the present study and their acronyms/schematics are noted in Figure 1. Zinc carbonate basic ($[ZnCO_3]_2{\cdot}[Zn(OH)_3]$),

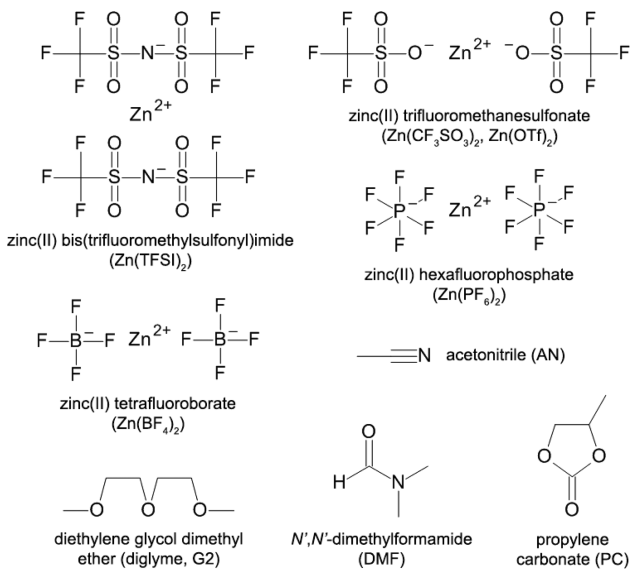

Figure 1. Structures and acronyms of the zinc salts and solvents studied.

tetrafluoroboric acid (HBF_4, 48 wt % in H_2O), zinc chloride ($ZnCl_2$), and silver hexafluorophosphate ($AgPF_6$) were purchased from Sigma-Aldrich and Alfar Aesar. The syntheses of $Zn(BF_4)_2$ and $Zn(PF_6)_2$ are following literature procedures.[46,47] A 2.75 g of zinc carbonate basic ($[ZnCO_3]_2{\cdot}[Zn(OH)_2]_3$, 25 mmol of Zn) was suspended in 250 mL of deionized water in a 500 mL round-bottom bottle, to which was added 8.2 g of tetrafluoroboric acid solution (HBF_4, 48 wt % in H_2O, 45 mmol of HBF_4) slowly over 30 min. After the bubbling stopped, the mixture was further stirred at room temperature overnight to confirm complete reaction. The mixture was then filtered through a Celite (Sigma-Aldrich) overnight. Removal of water solvent from the collected colorless solution via a Rotavapor evaporator afforded pure $Zn(BF_4)_2$ as white solid (4.0 g, 74.4% yield). The purity of salt was

DOI: 10.1021/acsami.5b10024
ACS Appl. Mater. Interfaces XXXX, XXX, XXX−XXX

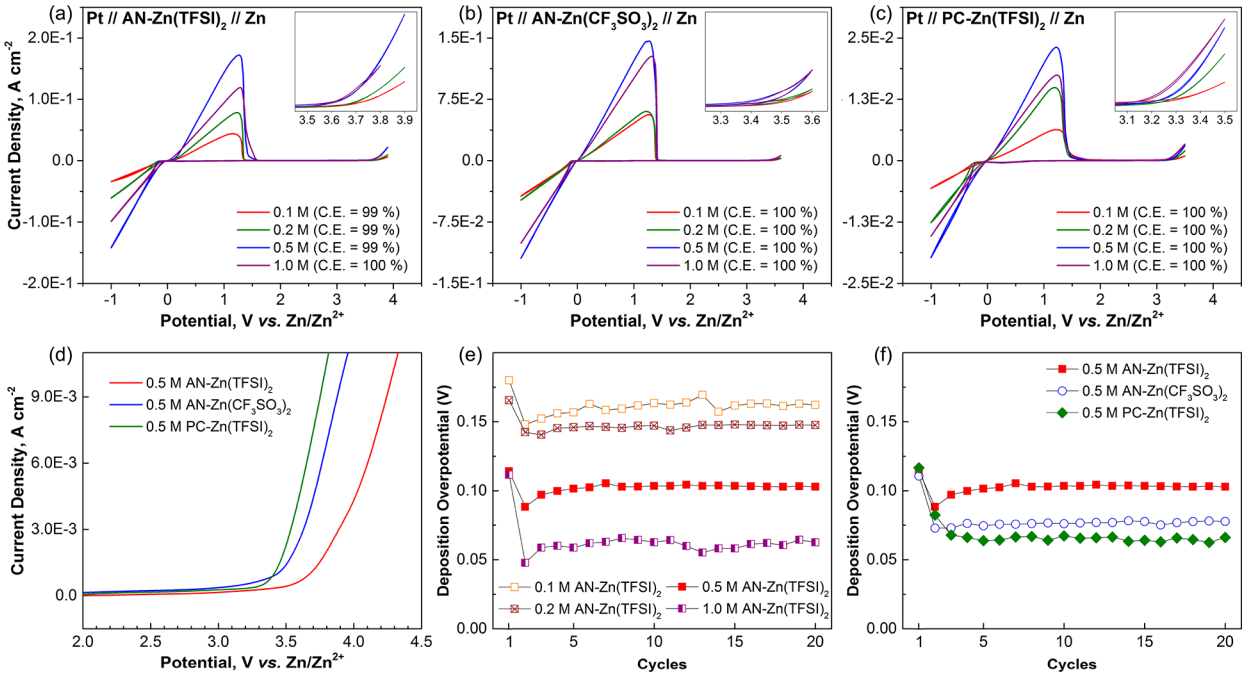

Figure 2. CVs of variable-concentration (a) AN−$Zn(TFSI)_2$, (b) AN−$Zn(CF_3SO_3)_2$, and (c) PC−$Zn(TFSI)_2$ (the scan rate for the CVs was 0.1 V s^{-1}). (d) LSVs of 0.5 M AN−$Zn(TFSI)_2$, AN−$Zn(CF_3SO_3)_2$, and PC−$Zn(TFSI)_2$ electrolytes (the scan rate for the LSVs was 0.025 V s^{-1}). Reversible deposition overpotential of (e) variable-concentration AN−$Zn(TFSI)_2$ and (f) 0.5 M AN−$Zn(TFSI)_2$, AN−$Zn(CF_3SO_3)_2$, and PC−$Zn(TFSI)_2$ electrolytes (the scan rate for the 20 CV cycles was 0.01 V s^{-1}).

confirmed by ^{19}F NMR in CH_3CN, recorded at −149.5 ppm, referenced to $Et_2O{\cdot}BF_3$ at −153 ppm. The salt was then dried under vacuum at room temperature overnight, which followed additional drying of $Zn(BF_4)_2$ at 80 °C under vacuum in an argon-filled glovebox for more than 24 h before use. In an argon-filled glovebox, 490 mg of zinc chloride ($ZnCl_2$, ≥98%, Sigma-Aldrich) (3.6 mmol of Zn) was suspended in 20 mL of anhydrous acetonitrile (CH_3CN, 99.8%, Sigma-Aldrich), to which was added a mixture, 1.77 g of silver hexafluorophosphate ($AgPF_6$, 98%, Sigma-Aldrich) (7.0 mmol of Ag) in 20 mL of anhydrous acetonitrile, slowly over 10 min. The mixture was allowed to stir at room temperature in the dark for 12 h to ensure the completion of the reaction. After stirring, the clear solution was collected via filtration through a Celite. Removal of acetonitrile from the solution under Schlenk line afforded white solid of analytically pure $Zn(PF_6)_2$ (430 mg, 34.6% yield). The salt was then dried under vacuum at room temperature in an argon-filled glovebox for more than 24 h before use.

$Zn(TFSI)_2$ (Solvionic, 99.5%) and $Zn(CF_3SO_3)_2$ (Sigma-Aldrich, 98%) were used after drying at 90 °C in a vacuum oven. Anhydrous diglyme (Sigma-Aldrich, 99.5%), propylene carbonate (Sigma-Aldrich, 99.7%), acetonitrile (Sigma-Aldrich, 99.8%), and *N*′,*N*′-dimethylformamide (Sigma-Aldrich, 99.8%) were used after overnight drying with completely dried molecular sieves (Sigma-Aldrich, 4 Å, 8−12 mesh). Appropriate ratios of zinc salts and solvents were mixed together in hermetically sealed glass vials and stirred on a hot plate to form homogeneous solutions. All materials were handled in an argon-filled inert atmosphere glovebox (<0.5 ppm of H_2O and <0.5 ppm of O_2). The water content of the mixtures was verified to be <30 ppm using a Mettler Toledo DL39 Karl Fischer coulometer.

Electrochemical Measurements and Morphology Characterization. Cyclic voltammetry (CV) and linear sweep voltammetry (LSV) measurements of the prepared electrolytes were performed in a three-electrode cell inside the glovebox using a Parstat MC potentiostat (Princeton Applied Research). The zinc wires (Alfa Aesar, 99.95%, 2.0 mm diameter) polished with a sand paper were used as the reference and the counter electrodes, and a Pt disk (CH Instruments, 2.0 mm diameter) was used as the working electrode. Conductivity values were measured in 20 °C steps from −20 to 60 °C using an Orion 3 Star conductivity meter (Thermo Scientific) with a MI-915 dip-type conductivity probe (Microelectrodes, Inc.), which is one of the integrated tools on Freeslate's robotic platform (CM3, Freeslate Inc.) in a custom-built nitrogen-filled glovebox (MB 200B, MBraun). In each measurement, the probe was washed with anhydrous methanol (Sigma-Aldrich, 99.8%) and dried over adsorbing mats to avoid cross contamination. The probe was regularly calibrated with standard solutions (0.1, 1, 5, 10, and 20 mS cm^{-1}, Ricca Chemical) at 25 °C. The error on the reported conductivities is estimated to be ±5%. The diffusion coefficient was estimated by the chronoamperometry technique using the same three-electrode cell used in CV or LSV measurements. The electrode potential was held at −0.5 V vs Zn/Zn^{2+} for 70 s. Current as a function of time was recorded using a Parstat MC potentiostat, and Coulombic charge was calculated by integrating current with respect to time. The diffusion coefficient was calculated according to the following equation:

$$Q = \frac{2nFAC_0D^{1/2}}{\pi^{1/2}}t^{1/2} + Q_{dl} + Q_{ads} \quad (1)$$

where Q is the total Coulombic charge (C) for Zn deposition, n is the number of electrons transferred, F is the Faraday constant (C mol^{-1}), A is the electrode area (cm^2), C_0 is the bulk Zn ion concentration (mol/cm^3), D is the Zn ion diffusion coefficient in the electrolyte (cm^2 s^{-1}), t is time (s), Q_{dl} is the double-layer charge, and Q_{ads} is the charge associated with the adsorbed species.[48]

Hitachi S4700 scanning electron microscope with an energy dispersive X-ray spectrometer (SEM-EDS) was used to characterize the morphology and to investigate the elements of deposited materials on a Pt electrode. To obtain deposited materials, chronopotentiometric technique was utilized for a Pt electrode in different nonaqueous Zn electrolytes at −0.5 mA constant current overnight.

MD Simulations and DFT Calculation. Classical molecular dynamics (MD) simulations were performed using the GROMACS MD simulation package, version 4.5.3.[49] Initial cubic simulation boxes with periodicity in the *XYZ* directions were constructed for the $Zn(TFSI)_2$ and $Zn(CF_3SO_3)_2$ salts in G2, AN, PC, and DMF solvents at 0.1 and 0.5 M concentrations using PACKMOL.[50] All initial configurations were subjected to two steps of energy minimization,

DOI: 10.1021/acsami.5b10024
ACS Appl. Mater. Interfaces XXXX, XXX, XXX−XXX

Table 1. Electrochemical Properties Comparison among 16 Different Nonaqueous Zn Electrolytes (for 0.1 M Concentration)

		$Zn(TFSI)_2$	$Zn(CF_3SO_3)_2$	$Zn(BF_4)_2$	$Zn(PF_6)_2$
diglyme (G2)	AS[a]	~2.6 V	~2.4 V	n/a	~2.3 V
	CE[b]	n/a	n/a	n/a	100%
	solubility[c]	lightly cloudy	homogeneous	not soluble	lightly cloudy
	CV[d]	additional redox reactions	additional redox reaction	n/a	additional redox reactions
acetonitrile (AN)	AS[a]	~3.8 V	~3.6 V	~3.8 V	~3.6 V
	CE[b]	99%	100%	100%	n/a
	solubility[c]	lightly cloudy	homogeneous	cloudy	homogeneous
	CV[d]	no additional redox reaction	no additional redox reaction	additional redox reactions	additional redox reactions
propylene carbonate (PC)	AS[a]	~3.4 V	~3.3 V	~3.3 V	~3.3 V
	CE[b]	100%	100%	n/a	100%
	solubility[c]	lightly cloudy	cloudy	cloudy	homogeneous
	CV[d]	additional redox reactions	additional redox reactions	additional redox reactions	additional redox reactions
N,*N*-dimethylformamide (DMF)	AS[a]	~2.9 V	~2.8 V	~2.8 V	~2.5 V
	CE[b]	50.8%	n/a	n/a	100%
	solubility[c]	lightly cloudy	homogeneous	cloudy	homogeneous
	CV[d]	additional redox reactions	additional redox reactions	additional redox reactions	additional redox reactions

[a]Anodic stability (V vs Zn/Zn^{2+}). [b]Coulombic efficiency. [c]At 25 °C (inhomogeneous mixtures with G2, AN, PC, and DMF were also stirred/heated on a hot plate up to 80−120 °C considering boiling point of each solvent and decomposition temperature of each salt, but transparent homogeneous solutions could not be created.) [d]Cyclic voltammogram.

first using steepest descent with the convergence criteria of 1000 kcal mol^{-1} $Å^{-1}$ followed by conjugated-gradient energy minimization with convergence criteria of 10 kcal mol^{-1} $Å^{-1}$. After minimization isothermal−isobaric (*NPT*) simulations were performed at 25 °C and 1 bar using the Berendsen barostat with a time constant of 0.1 ps to get the correct density. All systems were then heated to a temperature of 127 °C for 1 ns followed by a 3 ns annealing to 25 °C in a canonical ensemble (*NVT*) using an improved velocity rescaling algorithm with a coupling constant of 0.1 ps to ensure that the molecules were not trapped in a metastable state. Afterward, *NVT* simulations were performed for 10 ns to equilibrate the systems at 25 °C. The simulations are long enough to capture the structural and dynamical properties of equilibrated systems. Structural and dynamical properties were averaged over two independent configurations of the same system. The bonded and nonbonded parameters were obtained using generalized amber force fields (GAFF), and the partial charges were obtained with the RESP procedure using Antechamber.[51−53] Long range electrostatic interactions were handled by the particle-mesh Ewald (PME) method with a cutoff of 1.2 nm, and the Lennard-Jones interaction was truncated at 1.2 nm. The diffusion coefficient was computed from a least-squares fitting for a straight line in mean squared displacement in the diffusive regime. The conductivity is computed using the Nernst−Einstein (NE) equation as follows, where N_{pair} is the number of ion pairs, q_+ and $q-$ are the total charges on cation and anion respectively, D_+ and D_- are the self-diffusion coefficients of cation and anion, respectively, V is the simulation box volume, T is the temperature, k_β is the Boltzmann constant:

$$\sigma_{NE} = \frac{N_{pair}}{VTk_\beta}({q_+}^2 D_+ + {q_-}^2 D_-) \quad (2)$$

DFT calculations were performed using the QChem 4.1 package.[54,55] All the species were fully relaxed at the B3LYP/6-31+G* level.[56,57] Vibrational frequency calculations were carried out for each stationary point to check the character of the stationary point, as a true minimum should have no imaginary frequencies. All final geometries were confirmed as true minima by iteratively adjusting the structures. The single point energy was evaluated at the same theoretical level. The solvent effect is taken into account by the IEF-PCM dielectric continuum model.[58] All the calculations were carried out automatically by a workflow infrastructure developed by the Electrolyte Genome project.[59] Ionization potentials (IPs)[60](the energy to oxidize a compound as calculated by the energy difference between the oxidized and the original state) were calculated to predict the anodic stability of the electrolyte components. To identify the limiting components of the electrolyte electrochemical stability, we calculated the stability of both anions and solvents. Guided by the MD calculations, the anion IP calculation utilized the solvation structure of a Zn−anion ion pair for all systems except that of DMF−$Zn(TFSI)_2$, since ion pairing was found to be the prevailing solvation structure for the considered systems and concentrations.

RESULTS AND DISCUSSION

Zn Metal Plating/Stripping Behavior and Deposition Morphology. Parts a−c of Figure 2 represent the CVs of the AN−$Zn(TFSI)_2$, AN−$Zn(CF_3SO_3)_2$, and PC−$Zn(TFSI)_2$ electrolytes with varying concentration to evaluate the Zn plating/stripping behavior, Coulombic efficiency, overpotential, and the electrochemical window. In Figure 2a−c, the cathodic currents below 0 V and the anodic peak around the open-circuit voltage (OCV) are related to Zn deposition and dissolution, respectively.[23] The AN−$Zn(TFSI)_2$, AN−$Zn(CF_3SO_3)_2$, and PC−$Zn(TFSI)_2$ electrolytes show reversible Zn deposition behavior with negligible or no additional redox reaction and wide electrochemical window up to approximately 3.7, 3.5, and 3.4 V vs Zn/Zn^{2+}, respectively (Figure 2d, for 0.5 M concentration), suggesting that those mixtures can be used as potential electrolytes with a variety of cathode materials in rechargeable Zn batteries. It is noteworthy that all three electrolytes have the highest current density values for 0.5 M concentration (possibly due to increased unstable ion-paired anions[34] and/or solubility limit), which possibly can be selected as the standard concentration for further studies. Additional CVs and LSVs for the 0.1 M electrolytes composed of one of the zinc salts (i.e., $Zn(TFSI)_2$, $Zn(BF_4)_2$, $Zn(PF_6)_2$, and $Zn(CF_3SO_3)_2$) and one of the organic solvents (i.e., G2, PC, AN, and DMF) are demonstrated in Supporting Information (Figures S1−S4). In Figures S1−S4, the current density for several electrolytes exhibits minimal change on cycling (e.g., G2−$Zn(TFSI)_2$, G2−$Zn(CF_3SO_3)_2$, DMF−$Zn(BF_4)_2$, and DMF−$Zn(PF_6)_2$), possibly due to the reaction of the uncoordinated solvent present in the electrolyte with the freshly plated Zn metal.[61] Most other electrolytes, such as G2/DMF−$Zn(TFSI)_2$, G2/PC/DMF−$Zn(CF_3SO_3)_2$, AN/PC/DMF−$Zn(BF_4)_2$, and G2/AN/PC/DMF−$Zn(PF_6)_2$, also show the electrochemical plating/stripping behavior of Zn,

DOI: 10.1021/acsami.5b10024
ACS Appl. Mater. Interfaces XXXX, XXX, XXX−XXX

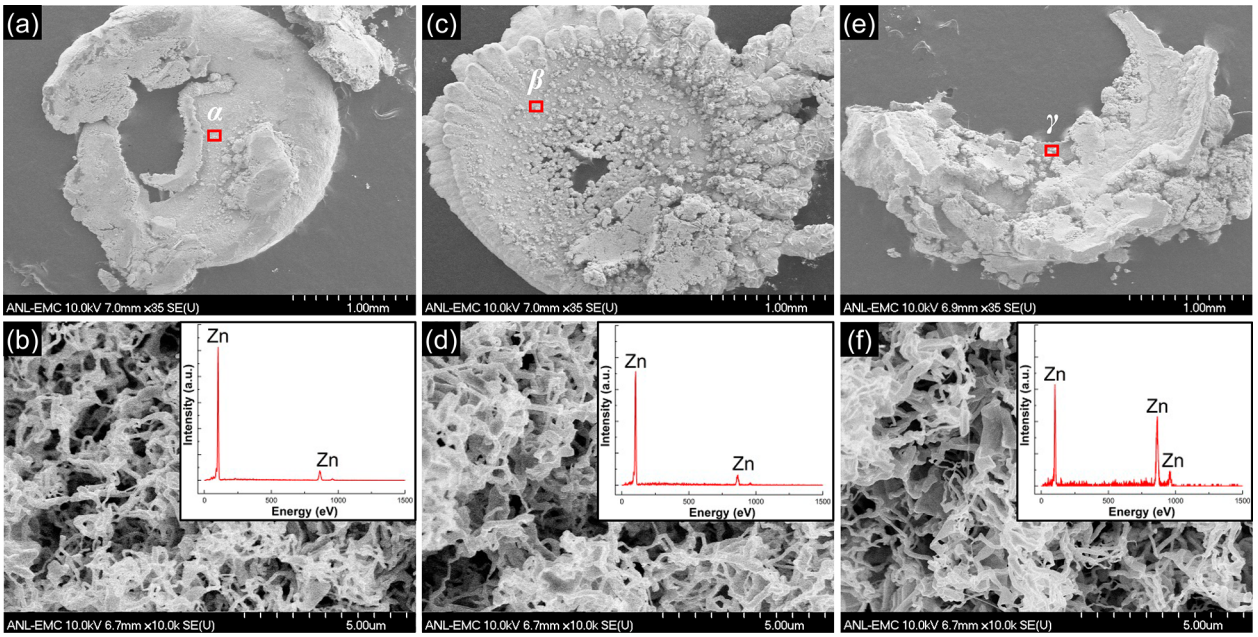

Figure 3. SEM images of (a) Pt electrode after overnight Zn deposition in 0.5 M AN−$Zn(TFSI)_2$ electrolyte, (b) a selected zone α of part a, (c) Pt electrode after overnight Zn deposition in 0.5 M AN−$Zn(CF_3SO_3)_2$ electrolyte, (d) a selected zone β of part c, (e) Pt electrode after overnight Zn deposition in 0.5 M PC−$Zn(TFSI)_2$ electrolyte, and (f) a selected zone γ of part e (the insets in parts b, d, and f show the EDS spectrum of Zn deposits).

but there are additional large and/or small peaks that indicate additional reversible and/or irreversible redox reactions. In addition, those electrolytes have relatively narrower electrochemical windows (Figures S1−S4). The CV of the G2−$Zn(BF_4)_2$ electrolyte is characterized by featureless cathodic and anodic currents, probably due to highly limited solubility of $Zn(BF_4)_2$ salt in G2, which can also be deduced from relatively low current density values (Figure S3a).

The Coulombic efficiency of Zn deposition/dissolution behavior from CVs is summarized in Table 1. Coulombic efficiency for most electrolytes is not available because the Zn plating/stripping peaks overlap with additional redox reaction peaks. Only 0.1 M DMF−$Zn(TFSI)_2$ electrolyte shows approximately 50.8 Coulombic efficiency, while other electrolytes, including the AN−$Zn(TFSI)_2$, PC−$Zn(TFSI)_2$, and AN−$Zn(CF_3SO_3)_2$ electrolytes, show ≥99% Coulombic efficiency for varying concentrations (Figure 2a−c), which suggests very high reversibility of Zn deposition/dissolution. Figure 2e and Figure 2f demonstrate the reversible deposition overpotential for the variable-concentration AN−$Zn(TFSI)_2$ electrolytes and the 0.5 M AN−$Zn(TFSI)_2$, AN−$Zn(CF_3SO_3)_2$, and PC−$Zn(TFSI)_2$ electrolytes, respectively. Additional results of reversible deposition overpotential for the variable-concentration AN−$Zn(CF_3SO_3)_2$ and PC−$Zn(TFSI)_2$ electrolytes are represented in Figure S5. After five cycles, the overpotential values are almost consistent for additional 15 cycles and are decreased with increase of concentration (Figures 2e and S5). In Figure 2f, the reversible deposition overpotential of 0.5 M AN−$Zn(TFSI)_2$ is the highest (~0.1 V), 0.5 M AN−$Zn(CF_3SO_3)_2$ the next (~0.07 V), and 0.5 M PC−$Zn(TFSI)_2$ the lowest (~0.06 V).

Typical SEM micrographs and the corresponding EDS spectrum of the deposited materials on the Pt electrodes are shown in Figure 3. Parts a, c, and e of Figure 3 provide overviews of the Zn deposited Pt electrodes in three selected nonaqueous Zn electrolytes (i.e., AN−$Zn(TFSI)_2$, AN−$Zn(CF_3SO_3)_2$, and PC−$Zn(TFSI)_2$) under a lower magnification, while parts b, d, and f of Figure 3 show the morphologies of selected zones (i.e., α, β, and γ) of each overview. The morphologies represent deposited Zn nanolines with approximately 100 nm diameter, which were possibly obtained from a nuclear-growth kinetic process of the Zn on the Pt electrodes. The inset images in parts b, d, and f of Figure 3 show the EDS spectrum for the deposited materials, in which $L\beta_1$, $K\alpha_1$, and $K\beta_1$ characteristic peaks at around 103.5, 863.7, and 957.0 eV, respectively, correspond to the Zn element. Both surface topography and EDS spectrum analysis indicate that only Zn is readily deposited on the Pt electrodes in all three selected electrolytes by utilizing chronopotentiometric technique, which is in accord with apparent Zn metal plating behavior observed from previous CVs (Figure 2). Upon the basis of the analysis of CVs and LSVs of the electrolytes (Figures 2 and S1−S4) and morphologies and EDS spectrum of the deposited materials (Figure 3), it appears that selected nonaqueous Zn electrolytes show highly efficient (≥99%) reversible deposition behavior on a Zn metal anode with wide electrochemical window (up to ~3.8 V vs Zn/Zn^{2+}), which can provide possible utilization of those electrolytes in nonaqueous Zn metal cells.

Electrochemical Stability and Elucidation of Its Limiting Factors. The oxidation of a nonaqueous electrolyte is a crucial issue when high potential cathodes are used for the development of high energy density batteries based on polar aprotic electrolyte solutions.[62] Most of the nonaqueous solvents and salts of interest are possibly oxidized at high potentials, and thus their intrinsic anodic behavior is important for further studies. The anodic stability of each 0.1 M electrolyte was obtained from LSVs measurements (Figures S1−S4) and summarized in Table 1. As shown in the CV plots (Figures S1b, S1c, and S2b), the LSVs confirm higher anodic stability of the 0.1 M AN−$Zn(TFSI)_2$, AN−$Zn(CF_3SO_3)_2$, and PC−$Zn(TFSI)_2$ electrolytes as 3.8, 3.6, and 3.4 V vs Zn/Zn^{2+}, respectively, compared to those of other electrolytes (Figures

DOI: 10.1021/acsami.5b10024
ACS Appl. Mater. Interfaces XXXX, XXX, XXX−XXX

S1–S4). It is noteworthy that anodic stability of an electrolyte reduces with increasing concentration (insets of Figure 2a–c): approximately 0.15 V for the AN–$Zn(TFSI)_2$, 0.1 V for the AN–$Zn(CF_3SO_3)_2$, and 0.17 V for the PC–$Zn(TFSI)_2$ electrolytes. In addition, it is interesting to note that a trend can be observed based on different solvents: the range of high voltage limit with varying Zn salts is approximately 3.6–3.8 V vs Zn/Zn^{2+} for AN, 3.3–3.4 V vs Zn/Zn^{2+} for PC, 2.5–2.9 V vs Zn/Zn^{2+} for DMF, and 2.3–2.6 V vs Zn/Zn^{2+} for G2 (Table 1). This indicates the following order for decreasing anodic stability in 0.1 M nonaqueous zinc electrolytes,

$$AN–Zn(X)_2 > PC–Zn(X)_2 > DMF–Zn(X)_2 \geq G2–Zn(X)_2$$
$$(X = TFSI^-, CF_3SO_3^-, BF_4^-, \text{and } PF_6^-)$$

which suggests that a solvent is one of the most important factors in determining the electrochemical window of nonaqueous Zn electrolytes.

The DFT predicted anodic stability (IP) is shown in Figure 4. In each electrolyte, the anodic stability limit is determined by

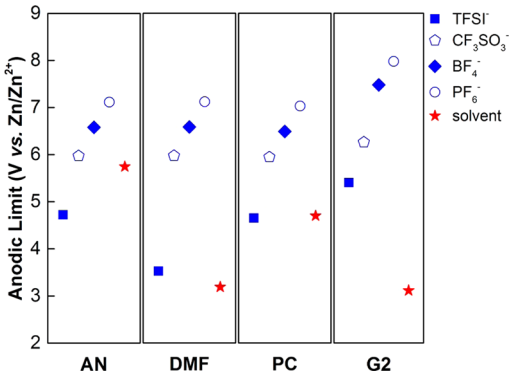

Figure 4. Calculated electrochemical windows (IP) of different salt anions in different solvent dielectric media. All the values are reported versus Zn/Zn^{2+}, and the solvent effect is taken into account by the IEF-PCM model. All the anions are listed in the legend and indicated by different symbols.

either the solvent or the anion, whichever is lower. For the 0.1 M AN–$Zn(TFSI)_2$, AN–$Zn(CF_3SO_3)_2$, and PC–$Zn(TFSI)_2$ electrolytes, the lowest anodic limit is above 4.0 V vs Zn/Zn^{2+}, which is roughly consistent with experimental results that no oxidation reaction is observed until approximately 3.8, 3.6, and 3.4 V vs Zn/Zn^{2+}, respectively. Except for the AN–$Zn(TFSI)_2$ and PC–$Zn(TFSI)_2$ electrolytes, the anions are predicted to have a higher anodic limit than the solvents. It means that the anodic stability of AN–$Zn(TFSI)_2$ and PC–$Zn(TFSI)_2$ electrolytes is mostly limited by the $TFSI^-$ anion, while the solvent is the predominant limiting factor for the anodic stability of the other electrolytes. The anodic stability of the electrolytes decreases in the order of AN ≥ PC > DMF ≥ G2, which is in good agreement with the experimental trend. Previous studies on anodic stability for a variety of nonaqueous systems highlight the salt, the electrode materials, and impurities as potential stability-limiting factors governing the onset of the oxidation reactions, but the anodic reactions of polar aprotic systems and their mechanism are unclear.[62] From our study of nonaqueous zinc electrolyte systems, it appears that the solvent is a dominant factor in determining the anodic stability, and only AN–$Zn(TFSI)_2$ and PC–$Zn(TFSI)_2$ are governed by the stability of the salt anion.

Ion Solvation and Ionic Association. The solvation structure (i.e., ion solvation and ionic association) is one of the important factors, as it provides a link between the molecular-level interactions and electrolyte properties such as diffusion coefficient and ionic conductivity. The Zn–anion, Zn–solvent, and anion–solvent radial distribution function $g(r)$, thus, was computed to understand the local solvation structure of the electrolyte. The $g(r)$ and snapshots of all computed systems are provided in Supporting Information (Figures S6–S13). The first solvation shell around Zn^{2+} consists of oxygen or nitrogen from $TFSI^-$ or $CF_3SO_3^-$ anion and/or solvent molecules at ~2.2 Å. The Zn–solvent $g(r)$ shows peak from Zn–O(DMF) and Zn–O(PC) at 2.2 Å and Zn–O(G2) at 2.1 Å, whereas Zn–N(AN) peak is observed at 2.3 Å (Figure S14). Among the four solvents considered in this work, small size O-donor solvents (i.e., DMF, PC, and G2) show the stronger interaction with Zn^{2+} as compared to N-donor solvents (i.e., AN), which indicates the following order of DMF > PC ~ G2 > AN for the strength of Zn–solvent interaction in the $Zn(TFSI)_2$ electrolytes and DMF ~ PC > G2 > AN in the $Zn(CF_3SO_3)_2$ electrolytes (Figure S14). Figure 5 shows the coordination

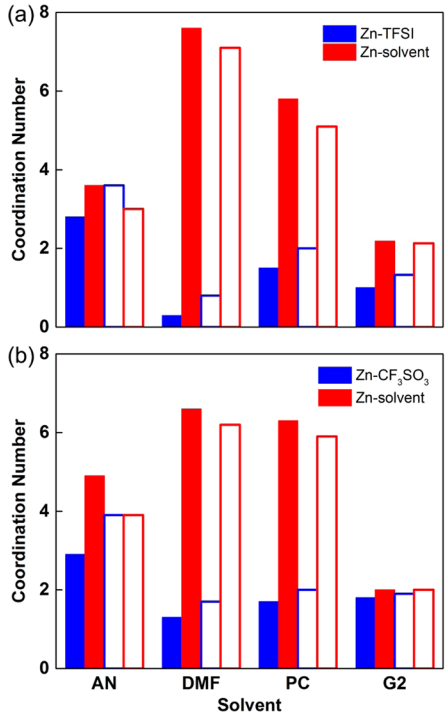

Figure 5. Coordination numbers of Zn–anion and Zn–solvent in the first solvation shell for the (a) $Zn(TFSI)_2$ and (b) $Zn(CF_3SO_3)_2$ electrolytes with four different solvents (0.1 M (filled bars) and 0.5 M (hollow bars) concentrations).

numbers (CN) of the Zn–anion and Zn–solvent for 0.1 and 0.5 M $Zn(TFSI)_2$ or $Zn(CF_3SO_3)_2$ electrolytes with DMF, PC, G2, and AN. The CN was computed by integrating $g(r)$ of atoms in their respective first solvation shell, which consists of oxygen or nitrogen from $TFSI^-$ or $CF_3SO_3^-$ anion and/or solvent molecules. For the Zn–anion coordination, the CN is computed by integrating $g(r)$ between Zn^{2+} and $N(TFSI^-)$ and Zn^{2+} and $S(CF_3SO_3^-)$, although the first solvation shell around Zn^{2+} consists of oxygen atoms of $TFSI^-$ and $CF_3SO_3^-$, while the CN in Zn–solvent coordination is computed from $g(r)$ between Zn^{2+} and N(AN), Zn^{2+} and O(DMF), Zn^{2+} and

DOI: 10.1021/acsami.5b10024
ACS Appl. Mater. Interfaces XXXX, XXX, XXX–XXX

O(PC), and Zn^{2+} and O(G2). The small size linear O-donor solvents exhibit better dissociating capability (between cations and anions) than the cyclic solvent of PC and N-donor solvent of AN. As previously reported for Mg electrolytes,[34] the dissociation of cation−anion is not directly proportional to dielectric constant of solvents: even though G2 has a much smaller dielectric constant, its high O-donor denticity and ability to wrap around cation promote dissociation between the cation and anion. Relatively weaker interaction between Zn^{2+} cations and AN solvent molecules results in formation of aggregates (AGGs) in the solution.

The increase in CNs of the Zn−anion and decrease in CNs of the Zn−solvent are observed with increasing concentration from 0.1 to 0.5 M (Figure 5). This increase in CNs of the Zn−anion with increasing concentration may affect the stability of an electrolyte if the ion-paired anions become unstable in the solution,[34] which can be observed in experimental results (Figure 2a−c). The decrease in CNs of the Zn−solvent with increasing concentration is the least for G2, which showcases its strong chelating effect around Zn^{2+} with high O-donor denticity. At both 0.1 and 0.5 M the CN of Zn−TFSI is similar to Zn−CF_3SO_3 in weakly coordinating solvents AN and PC, whereas CN of Zn−TFSI is smaller than ZN-CF_3SO_3 in strongly coordinating solvents DMF and G2. Also, the increase in CNs of Zn−TFSI and Zn−CF_3SO_3 with increase in concentration from 0.1 to 0.5 M is more significant in $TFSI^-$ as compared to $CF_3SO_3^-$. The molecular-level interactions between those solvent molecules and the anions were investigated to verify this difference. Figure S15 shows that in all solvents the $CF_3SO_3^-$ anions have relatively stronger interaction with solvent molecules as compared to $TFSI^-$ anions possibly due to the steric hindrance and more dispersed charge of the $TFSI^-$ anions resulting in lesser impact on Zn−CF_3SO_3 coordination with increase in concentration. Similar trends have been observed previously for lithium salts.[29,63] Upon the basis of the detailed understanding of electrolyte mixtures including how interactions at the molecular level are affected by factors such as solvent/ion structure and concentration, the relationship between the molecular-level interactions and electrolyte properties will be addressed in the following section.

Dynamical, Transport, Electrochemical Properties. The isothermal diffusion coefficients (at 25 °C) of the 0.1 M electrolytes composed of $Zn(TFSI)_2$ or $Zn(CF_3SO_3)_2$ salts with four different solvents (e.g., AN, DMF, PC, and G2) were estimated using eq 1 with the integrated values from chronoamperometry technique (Figure 6a) and were simulated from mean square displacement of ions (Figure 6b and Figure 6c). The trends observed in diffusion coefficient values from simulations are in good agreement with experimental results, while the quantitative agreement is difficult due to limitation of nonpolarizable force field used in this work. Among the four different solvent-based electrolytes, the AN-based electrolytes have the highest diffusion coefficient values and the DMF-based electrolytes show the second highest diffusion coefficient values compared to those of the PC- and G2-based electrolytes (Figure 6a). The MD simulations also indicate the same trend for the different solvents (Figure 6b and Figure 6c). It appears that a solvent with low viscosity, weaker coordination with Zn^{2+} and anions, such as AN, and more dispersed charge on salt anion, such as $TFSI^-$, may result in faster dynamics of both cation and anion. The mobility of cations and anions is the fastest in AN followed by DMF and the slowest in PC for both

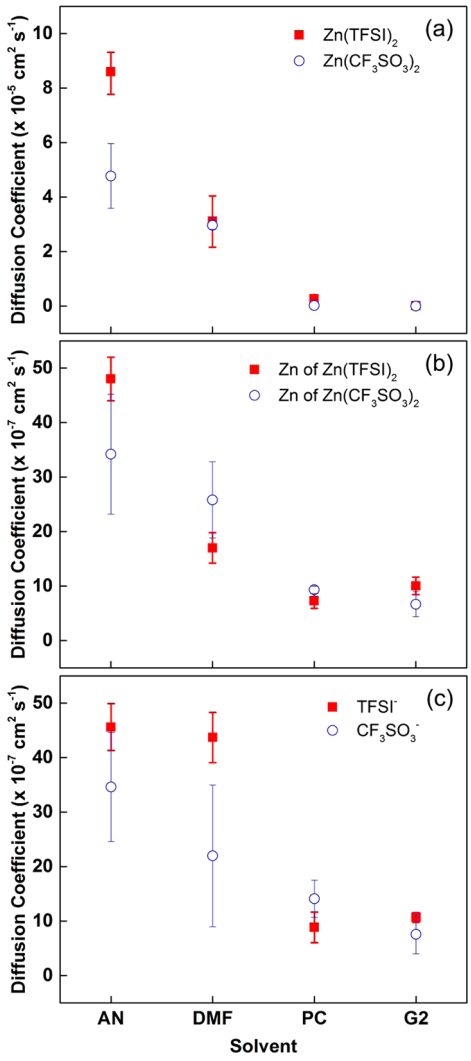

Figure 6. Isothermal diffusion coefficients of (a) $Zn(TFSI)_2$ and $Zn(CF_3SO_3)_2$ (from experimental estimation methods at 25 °C), (b) Zn^{2+} cations, and (c) $TFSI^-$ and $CF_3SO_3^-$ anions (from MD simulations at 25 °C, error bars were estimated based on the difference of the diffusion coefficients obtained from fits over the two halves of the fit interval) of 0.1 M $Zn(TFSI)_2$ and $Zn(CF_3SO_3)_2$ electrolytes with AN, DMF, PC, and G2.

$Zn(TFSI)_2$ and $Zn(CF_3SO_3)_2$ salts possibly due to viscosity difference (AN = 0.37 mPa·s, DMF = 0.79 mPa·s, and PC = 2.50 mPa·s at 25 °C) and dielectric constant difference (AN = 36.6, DMF = 38.3, and PC = 60 at 20 °C) in each solvent (Figure 6).[64,65] This trend is in agreement with previously reported experimental results for $LiClO_4$, where the fastest dynamics is observed in AN followed by DMF and the slowest dynamics in PC.[66] Upon the basis of the dynamics studies of AN-, DMF-, and PC-based electrolytes, it is concluded that relatively lower viscosity and dielectric constant of solvents result in faster dynamics of ions in the solution. Compared to PC, however, G2 has lower viscosity (1.88 mPa·s at 25 °C) and much lower dielectric constant (ε = 7.2 at 20 °C), but G2-based electrolyte shows similar ion mobility of PC-based electrolytes possibly due to its stronger chelating effect (Figure 6). In Figure 6b and Figure 6c, DMF has stronger interaction with Zn^{2+} of $Zn(TFSI)_2$ than Zn^{2+} of $Zn(CF_3SO_3)_2$, which contributes to more strongly solvated Zn^{2+} with slower dynamics and more uncoordinated $TFSI^-$ with faster dynamics.

DOI: 10.1021/acsami.5b10024
ACS Appl. Mater. Interfaces XXXX, XXX, XXX−XXX

In the case of AN-based electrolytes, the diffusion coefficient of Zn ion for $TFSI^-$ anion is relatively higher than that for $CF_3SO_3^-$ anion (Figure 6), probably due to an association tendency of the anions (i.e., anion···Zn^{2+} cation coordination) (uncoordinated free $TFSI^-$ anions, proposed to be a highly dissociated anions and also less coordinated with solvent molecules (Figure S15), result in higher diffusivity compared to highly associated $CF_3SO_3^-$ anions) reported in previous electrolyte solvation and ionic association studies for the AN−Li(X) electrolytes (X = PF_6^-, FSI^-, $TFSI^-$, ClO_4^-, $DFOB^-$, BF_4^-, $CF_3CO_2^-$, and $CF_3SO_3^-$).[28−33] Overall, all these observations in nonaqueous Zn electrolyte systems suggest that dynamics of ions are determined by a variety of complicated factors such as viscosity, dielectric constant, donor atoms of a solvent, molecular geometry, and strength of interaction with cation and anion.

The isothermal ionic conductivities (at 25 °C) of 0.1 M $Zn(TFSI)_2$ and $Zn(CF_3SO_3)_2$ electrolytes with AN, DMF, PC, and G2 were computed using eq 2 (Figure 7a). The trend in ionic conductivities (AN > DMF > PC ≥ G2) is in accordance with experimental results (Figure S16) and inferences from previous diffusion coefficient values (Figure 6). Faster dynamics and more charged pairs in AN-based electrolytes attribute to relatively higher conductivities compared to DMF-, PC-, and G2-based electrolytes. Figure 7b demonstrates the experimentally measured isothermal ionic conductivity values (at 20 °C) for the AN−$Zn(TFSI)_2$ electrolytes, along with values for the corresponding mixtures with another Zn salt (i.e., AN−$Zn(CF_3SO_3)_2$) or solvent (i.e., PC−$Zn(TFSI)_2$) for comparison. It is interesting to note that the AN− and PC−$Zn(TFSI)_2$ electrolytes exhibit a peak in ionic conductivity near the concentration of 0.5 M, which is not the case for other Li salt electrolytes with aprotic solvents,[30,67] while the ionic conductivity of the AN−$Zn(CF_3SO_3)_2$ electrolytes peaks near a concentration of 1.0 M (Figure 7b). The explanation for this may lie in possible increase of unstable ion-paired anions[34] and/or solubility limit with increasing concentration, noted above from solubility observation in Table 1: both AN− and PC−$Zn(TFSI)_2$ electrolytes are lightly cloudy solutions even at 0.1 M, while AN−$Zn(CF_3SO_3)_2$ electrolyte is a homogeneous solution. For the concentration range (0.1−1.0 M) at room temperature (20 °C), the conductivity of the AN−$Zn(TFSI)_2$ electrolyte is remarkably higher than the values for the electrolytes with another salt, $Zn(CF_3SO_3)_2$, or solvent, PC (Figure 7b), which may be expected considering the diffusion coefficient values for the AN−$Zn(TFSI)_2$ electrolyte in Figure 6. The variation with temperature of the ionic conductivities of the 0.5 M $Zn(TFSI)_2$ and $Zn(CF_3SO_3)_2$ electrolytes with four different solvents are given in Figure S16. Unlike other electrolytes, the ionic conductivities of the AN−$Zn(TFSI)_2$ and −$Zn(CF_3SO_3)_2$ electrolytes are almost the same or minor increase with increasing temperature (≥20 °C for the AN−$Zn(TFSI)_2$ and AN−$Zn(CF_3SO_3)_2$ electrolytes) possibly due to relatively lower boiling point of AN (82 °C). The behavior shown in Figure S16 for different solvents is in accord with the above-noted diffusion coefficient values for the electrolytes (Figure 6). The conductivity data were reproduced with samples prepared from different batches of Zn salts, and the water content of the electrolytes was verified to be negligible.

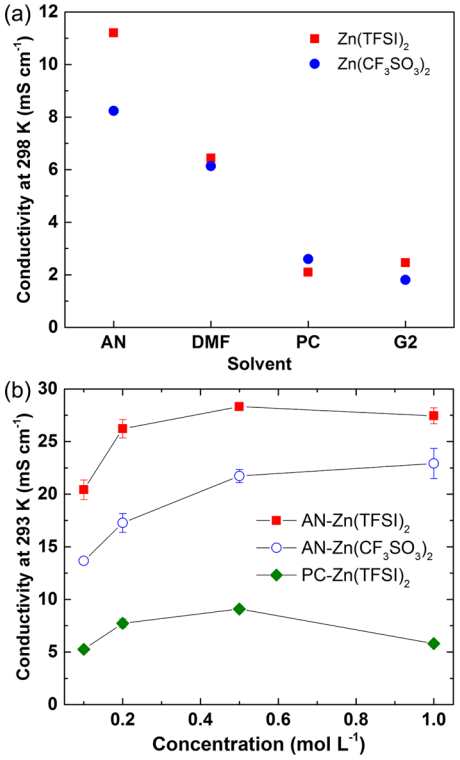

Figure 7. Isothermal ionic conductivities of (a) 0.1 M $Zn(TFSI)_2$ and $Zn(CF_3SO_3)_2$ electrolytes with AN, DMF, PC, and G2 (from MD simulations at 25 °C) and (b) the AN−$Zn(TFSI)_2$, AN−$Zn(CF_3SO_3)_2$, and PC−$Zn(TFSI)_2$ electrolytes with varying concentration (error bars shown for multiple measurements at 20 °C).

CONCLUSIONS

The electrochemical, transport, and dynamical properties of nonaqueous zinc electrolytes have been examined in detail by employing several modes of experimental evaluation in concert with MD simulations and DFT calculations. Among a variety of electrolytes, the AN−$Zn(TFSI)_2$, PC−$Zn(TFSI)_2$, and AN−$Zn(CF_3SO_3)_2$ electrolytes represent highly efficient (≥99%) reversible deposition behavior on a Zn metal anode with wide electrochemical window (up to 3.8 V vs Zn/Zn^{2+}), which can provide possible utilization of those electrolytes in nonaqueous zinc metal cells. Upon the basis of experimental analysis and DFT calculations for the anodic stability of electrolytes, we identify that the solvent is the most important factor in determining the anodic stability of most zinc electrolytes except for the case of $Zn(TFSI)_2$ where the $TFSI^-$ anion sets the upper voltage limit due to its relatively lower anodic stability. The solvation structure and dynamical/transport/electrochemical properties analyses demonstrate weakly coordinated nitrogen donor solvent, such as AN, promote formation of large complexes with faster dynamics and low partial charge which can dissociate easily resulting in higher conductivity. In the case of AN-based electrolytes, the diffusion coefficient of Zn ion for $TFSI^-$ anion, proposed to be a highly dissociated anion, is relatively higher than that for $CF_3SO_3^-$ anion, possibly highly associated anion, which results in relatively higher conductivity of the AN−$Zn(TFSI)_2$ electrolyte.

ASSOCIATED CONTENT

Supporting Information

The Supporting Information is available free of charge on the ACS Publications website at DOI: 10.1021/acsami.5b10024.

Additional experimental and simulation results (PDF)

DOI: 10.1021/acsami.5b10024
ACS Appl. Mater. Interfaces XXXX, XXX, XXX−XXX

AUTHOR INFORMATION

Corresponding Authors

*K.A.P.: e-mail, kapersson@lbl.gov.
*A.K.B.: e-mail, burrell@anl.gov.

Author Contributions

⊥S.-D.H. and N.N.R. contributed equally.

Notes

The authors declare no competing financial interest.

ACKNOWLEDGMENTS

This work was supported as part of the Joint Center for Energy Storage Research (JCESR), an Energy Innovation Hub funded by the U.S. Department of Energy, Office of Science, Basic Energy Sciences. The submitted manuscript has been created by UChicago Argonne, LLC, Operator of Argonne National Laboratory ("Argonne"). Argonne, a U.S. Department of Energy Office of Science laboratory, is operated under Contract DE-AC02-06CH11357. The U.S. Government retains for itself, and others acting on its behalf, a paid-up nonexclusive, irrevocable worldwide license in said article to reproduce, prepare derivative works, distribute copies to the public, and perform publicly and display publicly, by or on behalf of the Government. High performance computational resources for this research were provided by the National Energy Research Scientific Computing Center, which is supported by the Office of Science of the U.S. Department of Energy under Contract DE-AC02-05CH11231. The Materials Project (BES DOE Grant EDCBEE) is acknowledged for infrastructure and algorithmic support.

REFERENCES

(1) Xu, K. Nonaqueous Liquid Electrolytes for Lithium-Based Rechargeable Batteries. *Chem. Rev.* **2004**, *104*, 4303−4418.
(2) Simon, P.; Gogotsi, Y. Materials for Electrochemical Capacitors. *Nat. Mater.* **2008**, *7*, 845−854.
(3) Fergus, J. W. A Review of Electrolyte and Electrode Materials for High Temperature Electrochemical CO_2 and SO_2 Gas Sensors. *Sens. Actuators, B* **2008**, *134*, 1034−1041.
(4) Wang, Y.; Chen, K. S.; Mishler, J.; Cho, S. C.; Adroher, X. C. A Review of Polymer Electrolyte Membrane Fuel Cells: Technology, Applications, and Needs on Fundamental Research. *Appl. Energy* **2011**, *88*, 981−1007.
(5) Dimitrijević, S.; Rajčić-Vujasinović, M.; Trujić, V. Non-Cyanide Electrolytes for Gold Plating − A Review. *Int. J. Electrochem. Sci.* **2013**, *8*, 6620−6646.
(6) Xu, K. Electrolytes and Interphases in Li-Ion Batteries and Beyond. *Chem. Rev.* **2014**, *114*, 11503−11618.
(7) Zhong, C.; Deng, Y.; Hu, W.; Qiao, J.; Zhang, L.; Zhang, J. A Review of Electrolyte Materials and Compositions for Electrochemical Supercapacitors. *Chem. Soc. Rev.* **2015**, *44*, 7484−7539.
(8) Muldoon, J.; Bucur, C. B.; Gregory, T. Quest for Nonaqueous Multivalent Secondary Batteries: Magnesium and Beyond. *Chem. Rev.* **2014**, *114*, 11683−11720.
(9) Aurbach, D.; Lu, Z.; Schechter, A.; Gofer, Y.; Gizbar, H.; Turgeman, R.; Cohen, Y.; Moshkovich, M.; Levi, E. Prototype Systems for Rechargeable Magnesium Batteries. *Nature* **2000**, *407*, 724−727.
(10) Mizrahi, O.; Amir, N.; Pollak, E.; Chusid, O.; Marks, V.; Gottlieb, H.; Larush, L.; Zinigrad, E.; Aurbach, D. Electrolyte Solutions with a Wide Electrochemical Window for Rechargeable Magnesium Batteries. *J. Electrochem. Soc.* **2008**, *155*, A103−A109.
(11) Kim, H. S.; Arthur, T. S.; Allred, G. D.; Zajicek, J.; Newman, J. G.; Rodnyansky, A. E.; Oliver, A. G.; Boggess, W. C.; Muldoon, J. Structure and Compatibility of a Magnesium Electrolyte with a Sulphur Cathode. *Nat. Commun.* **2011**, *2*, 427.
(12) Liang, Y.; Feng, R.; Yang, S.; Ma, H.; Liang, J.; Chen, J. Rechargeable Mg Batteries with Graphene-like MoS_2 Cathode and Ultrasmall Mg Nanoparticle Anode. *Adv. Mater.* **2011**, *23*, 640−643.
(13) Muldoon, J.; Bucur, C. B.; Oliver, A. G.; Sugimoto, T.; Matsui, M.; Kim, H. S.; Allred, G. D.; Zajicek, J.; Kotani, Y. Electrolyte Roadblocks to a Magnesium Rechargeable Battery. *Energy Environ. Sci.* **2012**, *5*, 5941−5950.
(14) Guo, Y.-S.; Zhang, F.; Yang, J.; Wang, F.-F.; NuLi, Y.; Hirano, S.-I. Boron-Based Electrolyte Solutions with Wide Electrochemical Windows for Rechargeable Magnesium Batteries. *Energy Environ. Sci.* **2012**, *5*, 9100−9106.
(15) Wang, F. F.; Guo, Y. S.; Yang, J.; Nuli, Y.; Hirano, S.-I. A Novel Electrolyte System without a Grignard Reagent for Rechargeable Magnesium Batteries. *Chem. Commun.* **2012**, *48*, 10763−10765.
(16) Mohtadi, R.; Matsui, M.; Arthur, T. S.; Hwang, S.-J. Magnesium Borohydride: From Hydrogen Storage to Magnesium Battery. *Angew. Chem., Int. Ed.* **2012**, *51*, 9780−9783.
(17) Muldoon, J.; Bucur, C. B.; Oliver, A. G.; Zajicek, J.; Allred, G. D.; Boggess, W. C. Corrosion of Magnesium Electrolytes: Chlorides—The Culprit. *Energy Environ. Sci.* **2013**, *6*, 482−487.
(18) Yoo, H. D.; Shterenberg, I.; Gofer, Y.; Gershinsky, G.; Pour, N.; Aurbach, D. Mg Rechargeable Batteries: an On-Going Challenge. *Energy Environ. Sci.* **2013**, *6*, 2265−2279.
(19) Barile, C. J.; Spatney, R.; Zavadil, K. R.; Gewirth, A. A. Investigating the Reversibility of in Situ Generated Magnesium Organohaloaluminates for Magnesium Deposition and Dissolution. *J. Phys. Chem. C* **2014**, *118*, 10694−10699.
(20) Carter, T. J.; Mohtadi, R.; Arthur, T. S.; Mizuno, F.; Zhang, R.; Shirai, S.; Kampf, J. W. Boron Clusters as Highly Stable Magnesium-Battery Electrolytes. *Angew. Chem., Int. Ed.* **2014**, *53*, 3173−3177.
(21) Bucur, C. B.; Gregory, T.; Muldoon, J. In *Rechargeable Batteries: Materials, Technologies and New Trends*; Zhang, Z., Zhang, S. S., Eds.; Springer International Publishing: Switzerland, 2015; Chapter 22, pp 611−635.
(22) Ha, S.-Y.; Lee, Y.-W.; Woo, S. W.; Koo, B.; Kim, J.-S.; Cho, J.; Lee, K. T.; Choi, N.-S. Magnesium(II) Bis(trifluoromethane sulfonyl) Imide-Based Electrolytes with Wide Electrochemical Windows for Rechargeable Magnesium Batteries. *ACS Appl. Mater. Interfaces* **2014**, *6*, 4063−4073.
(23) Aurbach, D.; Skaletsky, R.; Gofer, Y. The Electrochemical Behavior of Calcium Electrodes in a Few Organic Electrolytes. *J. Electrochem. Soc.* **1991**, *138*, 3536−3545.
(24) Ponrouch, A.; Frontera, C.; Bardé, F.; Palacín, M. R. Towards a Calcium-Based Rechargeable Battery. *Nat. Mater.* **2016**, *15*, 169−172, DOI: 10.1038/nmat4462.
(25) Ellingham, H. J. T. Reducibility of Oxides and Sulphides in Metallurgical Processes. *J. Soc. Chem. Ind.* **1944**, *63*, 125−133.
(26) Rong, Z.; Malik, R.; Canepa, P.; Gautam, G. S.; Liu, M.; Jain, A.; Persson, K.; Ceder, G. Materials Design Rules for Multivalent Ion Mobility in Intercalation Structures. *Chem. Mater.* **2015**, *27*, 6016−6021.
(27) Shannon, R. D. Revised Effective Ionic Radii and Systematic Studies of Interatomic Distances in Halides and Chalcogenides. *Acta Crystallogr., Sect. A: Cryst. Phys., Diffr., Theor. Gen. Crystallogr.* **1976**, *A32*, 751−767.
(28) Seo, D. M.; Borodin, O.; Han, S.-D.; Ly, Q.; Boyle, P. D.; Henderson, W. A. Electrolyte Solvation and Ionic Association I. Acetonitrile-Lithium Salt Mixtures: Intermediate and Highly Associated Salts. *J. Electrochem. Soc.* **2012**, *159*, A553−A565.
(29) Seo, D. M.; Borodin, O.; Han, S.-D.; Boyle, P. D.; Henderson, W. A. Electrolyte Solvation and Ionic Association II. Acetonitrile-Lithium Salt Mixtures: Highly Dissociated Salts. *J. Electrochem. Soc.* **2012**, *159*, A1489−A1500.
(30) Seo, D. M.; Borodin, O.; Balogh, D.; O'Connell, M.; Ly, Q.; Han, S.-D.; Passerini, S.; Henderson, W. A. Electrolyte Solvation and Ionic Association III. Acetonitrile-Lithium Salt Mixtures—Transport Properties. *J. Electrochem. Soc.* **2013**, *160*, A1061−A1070.
(31) Han, S.-D.; Borodin, O.; Allen, J. L.; Seo, D. M.; McOwen, D. W.; Yun, S.-H.; Henderson, W. A. Electrolyte Solvation and Ionic

DOI: 10.1021/acsami.5b10024
ACS Appl. Mater. Interfaces XXXX, XXX, XXX−XXX

Association IV. Acetonitrile-Lithium Difluoro(oxalato)borate (LiDFOB) Mixtures. *J. Electrochem. Soc.* **2013**, *160*, A2100−A2110.
(32) Han, S.-D.; Borodin, O.; Seo, D. M.; Zhou, Z.-B.; Henderson, W. A. Electrolyte Solvation and Ionic Association V. Acetonitrile-Lithium Bis(fluorosulfonyl)imide (LiFSI) Mixtures. *J. Electrochem. Soc.* **2014**, *161*, A2042−A2053.
(33) Borodin, O.; Han, S.-D.; Daubert, J. S.; Seo, D. M.; Yun, S.-H.; Henderson, W. A. Electrolyte Solvation and Ionic Association VI. Acetonitrile-Lithium Salt Mixtures: Highly Associated Salts Revisited. *J. Electrochem. Soc.* **2015**, *162*, A501−A510.
(34) Rajput, N. N.; Qu, X.; Sa, N.; Burrell, A. K.; Persson, K. A. The Coupling between Stability and Ion Pair Formation in Magnesium Electrolytes from First-Principles Quantum Mechanics and Classical Molecular Dynamics. *J. Am. Chem. Soc.* **2015**, *137*, 3411−3420.
(35) Xu, C.; Du, H.; Li, B.; Kang, F.; Zeng, Y. Reversible Insertion Properties of Zinc Ion into Manganese Dioxide and Its Application for Energy Storage. *Electrochem. Solid-State Lett.* **2009**, *12*, A61−A65.
(36) Xu, C.; Li, B.; Du, H.; Kang, F. Energetic Zinc Ion Chemistry: The Rechargeable Zinc Ion Battery. *Angew. Chem., Int. Ed.* **2012**, *51*, 933−935.
(37) Xu, C.; Chiang, S. W.; Ma, J.; Kang, F. Investigation on Zinc Ion Storage in Alpha Manganese Dioxide for Zinc Ion Battery by Electrochemical Impedance Spectrum. *J. Electrochem. Soc.* **2013**, *160*, A93−A97.
(38) Lee, J.; Ju, J. B.; Cho, W. I.; Cho, B. W.; Oh, S. H. Todorokite-Type MnO_2 as a Zinc-Ion Intercalating Material. *Electrochim. Acta* **2013**, *112*, 138−143.
(39) Lee, B.; Yoon, C. S.; Lee, H. R.; Chung, K. Y.; Cho, B. W.; Oh, S. H. Electrochemically-Induced Reversible Transition from the Tunneled to Layered Polymorphs of Manganese Dioxide. *Sci. Rep.* **2014**, *4*, 6066.
(40) Jia, Z.; Wang, B.; Wang, Y. Copper Hexacyanoferrate with a Well-Defined Open Framework as a Positive Electrode for Aqueous Zinc Ion Batteries. *Mater. Chem. Phys.* **2015**, *149*−*150*, 601−606.
(41) Trócoli, R.; La Mantia, F. An Aqueous Zinc-Ion Battery Based on Copper Hexacyanoferrate. *ChemSusChem* **2015**, *8*, 481−485.
(42) Gocke, E.; Schramm, W.; Dolscheid, P.; Schöllhorn, R. Molybdenum Cluster Chalcogenides Mo_6X_8: Electrochemical Intercalation of Closed Shell Ions Zn^{2+}, Cd^{2+}, and Na^+. *J. Solid State Chem.* **1987**, *70*, 71−81.
(43) Venkata Narayanan, N. S.; Ashokraj, B. V.; Sampath, S. Ambient Temperature, Zinc Ion-Conducting, Binary Molten Electrolyte Based on Acetamide and Zinc Perchlorate: Application in Rechargeable Zinc Batteries. *J. Colloid Interface Sci.* **2010**, *342*, 505−512.
(44) Simons, T. J.; MacFarlane, D. R.; Forsyth, M.; Howlett, P. C. Zn Electrochemistry in 1-Ethyl-3-Methylimidazolium and *N*-Butyl-*N*-Methylpyrrolidinium Dicyanamides: Promising New Rechargeable Zn Battery Electrolytes. *ChemElectroChem* **2014**, *1*, 1688−1697.
(45) Guerfi, A.; Trottier, J.; Boyano, I.; De Meatza, I.; Blazquez, J. A.; Brewer, S.; Ryder, K. S.; Vijh, A.; Zaghib, K. High Cycling Stability of Zinc-Anode/Conducting Polymer Rechargeable Battery with Non-Aqueous Electrolyte. *J. Power Sources* **2014**, *248*, 1099−1104.
(46) Proffit, D. L.; Lipson, A. L.; Pan, B.; Han, S.-D.; Fister, T. T.; Feng, Z.; Ingram, B. J.; Burrell, A. K.; Vaughey, J. T. Reducing Side Reactions Using PF_6-based Electrolytes in Multivalent Hybrid Cells. *MRS Online Proc. Libr.* **2015**, *1773*, 27−32.
(47) Lipson, A. L.; Proffit, D. L.; Pan, B.; Fister, T. T.; Liao, C.; Burrell, A. K.; Vaughey, J. T.; Ingram, B. J. Current Collector Corrosion in Ca-Ion Batteries. *J. Electrochem. Soc.* **2015**, *162*, A1574−A1578.
(48) Anson, F. C. Innovations in the Study of Adsorbed Reactants by Chronocoulometry. *Anal. Chem.* **1966**, *38*, 54−57.
(49) Pronk, S.; Páll, S.; Schulz, R.; Larsson, P.; Bjelkmar, P.; Apostolov, R.; Shirts, M. R.; Smith, J. C.; Kasson, P. M.; van der Spoel, D.; Hess, B.; Lindahl, E. GROMACS 4.5: A High-Throughput and Highly Parallel Open Source Molecular Simulation Toolkit. *Bioinformatics* **2013**, *29*, 845−854.
(50) Martínez, L.; Andrade, R.; Birgin, E. G.; Martínez, J. M. PACKMOL: A Package for Building Initial Configurations for Molecular Dynamics Simulations. *J. Comput. Chem.* **2009**, *30*, 2157−2164.
(51) Wang, J.; Wolf, R. M.; Caldwell, J. W.; Kollman, P. A.; Case, D. A. Development and Testing of a General Amber Force Field. *J. Comput. Chem.* **2004**, *25*, 1157−1174.
(52) Wang, J.; Wang, W.; Kollman, P. A.; Case, D. A. Automatic Atom Type and Bond Type Perception in Molecular Mechanical Calculations. *J. Mol. Graphics Modell.* **2006**, *25*, 247−260.
(53) Bayly, C. I.; Cieplak, P.; Cornell, W. D.; Kollman, P. A. A Well-Behaved Electrostatic Potential Based Method Using Charge Restraints for Deriving Atomic Charges: The RESP Model. *J. Phys. Chem.* **1993**, *97*, 10269−10280.
(54) Shao, Y.; Gan, Z.; Epifanovsky, E.; Gilbert, A. T. B.; Wormit, M.; Kussmann, J.; Lange, A. W.; Behn, A.; Deng, J.; Feng, X.; Ghosh, D.; Goldey, M.; Horn, P. R.; Jacobson, L. D.; Kaliman, I.; Khaliullin, R. Z.; Kuś, T.; Landau, A.; Liu, J.; Proynov, E. I.; Rhee, Y. M.; Richard, R. M.; Rohrdanz, M. A.; Steele, R. P.; Sundstrom, E. J.; Woodcock, H. L., III; Zimmerman, P. M.; Zuev, D.; Albrecht, B.; Alguire, E.; Austin, B.; Beran, G. J. O.; Bernard, Y. A.; Berquist, E.; Brandhorst, K.; Bravaya, K. B.; Brown, S. T.; Casanova, D.; Chang, C.-M.; Chen, Y.; Chien, S. H.; Closser, K. D.; Crittenden, D. L.; Diedenhofen, M.; DiStasio, R. A., Jr.; Do, H.; Dutoi, A. D.; Edgar, R. G.; Fatehi, S.; Fusti-Molnar, L.; Ghysels, A.; Golubeva-Zadorozhnaya, A.; Gomes, J.; Hanson-Heine, M. W. D.; Harbach, P. H. P.; Hauser, A. W.; Hohenstein, E. G.; Holden, Z. C.; Jagau, T.-C.; Ji, H.; Kaduk, B.; Khistyaev, K.; Kim, J.; Kim, J.; King, R. A.; Klunzinger, P.; Kosenkov, D.; Kowalczyk, T.; Krauter, C. M.; Lao, K. U.; Laurent, A.; Lawler, K. V.; Levchenko, S. V.; Lin, C. Y.; Liu, F.; Livshits, E.; Lochan, R. C.; Luenser, A.; Manohar, P.; Manzer, S. F.; Mao, S.-P.; Mardirossian, N.; Marenich, A. V.; Maurer, S. A.; Mayhall, N. J.; Neuscamman, E.; Oana, C. M.; Olivares-Amaya, R.; O'Neill, D. P.; Parkhill, J. A.; Perrine, T. M.; Peverati, R.; Prociuk, A.; Rehn, D. R.; Rosta, E.; Russ, N. J.; Sharada, S. M.; Sharma, S.; Small, D. W.; Sodt, A.; Stein, T.; Stück, D.; Su, Y.-C.; Thom, A. J. W.; Tsuchimochi, T.; Vanovschi, V.; Vogt, L.; Vydrov, O.; Wang, T.; Watson, M. A.; Wenzel, J.; White, A.; Williams, C. F.; Yang, J.; Yeganeh, S.; Yost, S. R.; You, Z.-Q.; Zhang, I. Y.; Zhang, X.; Zhao, Y.; Brooks, B. R.; Chan, G. K. L.; Chipman, D. M.; Cramer, C. J.; Goddard, W. A., III; Gordon, M. S.; Hehre, W. J.; Klamt, A.; Schaefer, H. F., III; Schmidt, M. W.; Sherrill, C. D.; Truhlar, D. G.; Warshel, A.; Xu, X.; Aspuru-Guzik, A.; Baer, R.; Bell, A. T.; Besley, N. A.; Chai, J.-D.; Dreuw, A.; Dunietz, B. D.; Furlani, T. R.; Gwaltney, S. R.; Hsu, C.-P.; Jung, Y.; Kong, J.; Lambrecht, D. S.; Liang, W.; Ochsenfeld, C.; Rassolov, V. A.; Slipchenko, L. V.; Subotnik, J. E.; Van Voorhis, T.; Herbert, J. M.; Krylov, A. I.; Gill, P. M. W.; Head-Gordon, M. Advances in Molecular Quantum Chemistry Contained in the Q-Chem 4 Program Package. *Mol. Phys.* **2015**, *113*, 184−215.
(55) Krylov, A. I.; Gill, P. M. W. Q-Chem: An Engine for Innovation. *Wiley Interdiscip. Rev. Comput. Mol. Sci.* **2013**, *3*, 317−326.
(56) Stephens, P. J.; Devlin, F. J.; Chabalowski, C. F.; Frisch, M. J. Ab Initio Calculation of Vibrational Absorption and Circular Dichroism Spectra Using Density Functional Force Fields. *J. Phys. Chem.* **1994**, *98*, 11623−11627.
(57) Ditchfield, R.; Hehre, W. J.; Pople, J. A. Self-Consistent Molecular-Orbital Methods. IX. An Extended Gaussian-Type Basis for Molecular-Orbital Studies of Organic Molecules. *J. Chem. Phys.* **1971**, *54*, 724−728.
(58) Tomasi, J.; Mennucci, B.; Cancès, E. The IEF Version of the PCM Solvation Method: An Overview of a New Method Addressed to Study Molecular Solutes at the QM Ab Initio Level. *J. Mol. Struct.: THEOCHEM* **1999**, *464*, 211−226.
(59) Qu, X.; Jain, A.; Rajput, N. N.; Cheng, L.; Zhang, Y.; Ong, S. P.; Brafman, M.; Maginn, E.; Curtiss, L. A.; Persson, K. A. The Electrolyte Genome Project: A Big Data Approach in Battery Materials Discovery. *Comput. Mater. Sci.* **2015**, *103*, 56−67.
(60) Ong, S. P.; Andreussi, O.; Wu, Y.; Marzari, N.; Ceder, G. Electrochemical Windows of Room-Temperature Ionic Liquids from Molecular Dynamics and Density Functional Theory Calculations. *Chem. Mater.* **2011**, *23*, 2979−2986.

DOI: 10.1021/acsami.5b10024
ACS Appl. Mater. Interfaces XXXX, XXX, XXX−XXX

(61) Qian, J.; Henderson, W. A.; Xu, W.; Bhattacharya, P.; Engelhard, M.; Borodin, O.; Zhang, J.-G. High Rate and Stable Cycling of Lithium Metal Anode. *Nat. Commun.* **2015**, *6*, 6362.
(62) Aurbach, D.; Gofer, Y. In *Nonaqueous Electrochemistry*; Aurbach, D., Eds.; Marcel Dekker, Inc.: New York, NY, 1999; Chapter 4, pp 195−212.
(63) Henderson, W. A. Glyme−Lithium Salt Phase Behavior. *J. Phys. Chem. B* **2006**, *110*, 13177−13183.
(64) Lide, D. R. *CRC Handbook of Chemistry and Physics*, 85th ed; CRC Press LLC: Boca Raton, FL, 2004.
(65) Wohlfarth, C. *Landolt-Börnstein IV/25: Viscosity of Pure Organic Liquids and Binary Liquid Mixtures*; Lechner, M. D., Ed.; Springer: Berlin, 2009.
(66) Sullivan, J. M.; Hanson, D. C.; Keller, R. Diffusion Coefficients in Propylene Carbonate, Dimethyl Formamide, Acetonitrile, and Methyl Formate. *J. Electrochem. Soc.* **1970**, *117*, 779−780.
(67) Ding, M. S. Conductivity and Viscosity of PC-DEC and PC-EC Solutions of $LiBF_4$. *J. Electrochem. Soc.* **2004**, *151*, A40−A47.

DOI: 10.1021/acsami.5b10024
ACS Appl. Mater. Interfaces XXXX, XXX, XXX−XXX